Electromagnetically-Induced Vibration in Particulate-Functionalized Materials

T. I. Zohdi
Department of Mechanical Engineering,
6195 Etcheverry Hall,
University of California,
Berkeley, CA, 94720-1740

In many small-scale devices, the materials employed are functionalized (doped) with microscale and/or nanoscale particles, in order to deliver desired overall dielectric properties. In this work, we develop a reduced-order lumped-mass model to characterize the dynamic response of a material possessing a microstructure that is comprised of an electromagnetically-neutral binder with embedded electromagnetically-sensitive (charged) particles. In certain industrial applications, such materials may encounter external electrical loading that can be highly oscillatory. Therefore, it is possible for the forcing frequencies to activate the inherent resonant frequencies of these micro- and nanostructures. In order to extract qualitative information, this paper first analytically investigates the mechanical and electromagnetic (cyclotronic) contributions to the dynamic response for a single particle, and then quantitatively investigates the response of a model problem consisting of a coupled multiparticle periodic array, via numerical simulation, using an implicit temporally-adaptive trapezoidal time-stepping scheme. For the model problem, numerical studies are conducted to observe the cyclotronically-dominated resonant frequency and associated beat phenomena, which arises due to the presence of mechanical and electromagnetic harmonics in the material system.
[DOI: 10.1115/1.4023251]

Keywords: particulate composites, electromagnetics, vibration

1 Introduction and Objectives

The motivation for this analysis is the functionalization of materials by the introduction of small-scale particles into a base material, as shown in Fig. 1. The specific materials of interest are comprised of an electrically-neutral binding material that is easy to form and electromagnetically-sensitive (charged) particles that are used to modify the overall response of the material to achieve a desired effect. The scientific analysis of materials with a particle-laden microstructure dates back at least to Maxwell [1,2], and Lord Rayleigh [3]. For an extensive overview of the field, see Torquato [4], while for more mathematical aspects, see Jikov et al. [5], for solid-mechanics oriented analyses see Hashin [6], Markov [7], Mura [8], Nemat-Nasser and Hori [9], Huet [10,11], and for computational aspects see Zohdi and Wriggers [12], Zohdi [13] and, recently, Ghosh [14], Ghosh and Dimiduk [15]. Applications for such materials are driven by the extensive sensor, actuator, and MEMS industries. For specific applications, see Rebeiz et al. [16], Quandt and Ludwig [17], Grimes et al. [18], and Kouzoudis and Grimes [19,20], Azevedo et al. [21], Jones et al. [22], and Myers et al. [23]. In certain instances, these materials are used in conjunction with static magnetic fields to facilitate devices which handle time-varying electrical loads. In these cases, on-chip magnets (permanent, passive, inductors) have become critical in the continuous miniaturization, and the reduction of available chip layout area, of electronic devices. We refer the reader to Yamaguchi et al. [24,25,26], Zhuang et al. [27–29], Kim et al. [30], Gardner et al. [31,32], Viala et al. [33,34], Xu et al. [35], Jiang et al. [36], Ikeda et al. [37], Zhao et al. [38], Hsu et al. [39], Salvia et al. [40], Rosselle et al. [41], and Wallace [42] for a cross-sectional view of the field.

Because the external electrical loads are highly oscillatory, it is possible for the forcing frequencies to approach the resonant frequencies of these micro- and nanostructures, or to exhibit vibrational characteristics that can eventually lead to device breakdown. With this issue as a motivation, this paper develops a reduced-order lumped-mass model to characterize the dynamics of particle groups that are bound to an electromagnetically-neutral medium, in the presence of and externally-controlled electromagnetic field, $\mathbf{B}^{\text{ext}}$ and $\mathbf{E}^{\text{ext}}$. Specifically, the i^{th} particle in a collection of charged particles $i = 1, 2, ..., N_p$ is governed by a balance of forces

$$m_i \dot{v}_i = q_i(\boldsymbol{E}^{\text{ext}} + v_i \times \boldsymbol{B}^{\text{ext}}) + \sum_{j \neq i}^{N} \boldsymbol{\Psi}_{ij} + \boldsymbol{\Psi}_i^b \tag{1}$$

where m_i is the particle mass, v_i is the particle velocity, q_i is the charge of the particle, $\boldsymbol{\Psi}_{ij}$ represents the interaction of the particle with all other particles in the system and $\boldsymbol{\Psi}_i^b$ represents the binding force between the particle and the surrounding medium. In this reduced-order model, the only role of the binding medium is to tether the particles to their original equilibrium (at $t = 0$) positions. The analysis proceeds as follows:

- First, in order to extract qualitative system behavior, an analytical investigation of the response of an isolated particle in an oscillatory electric and static magnetic field bound is initially undertaken.
- Second, in order to extract quantitative characteristics of coupled multiparticle systems, a numerical analysis is undertaken. The paper concludes with a discussion of the possible continuum modeling extensions for these types of systems.

2 Qualitative Analysis: Motion of a Single Particle

Before addressing the full-blown, multiparticle coupled system under oscillatory electric and static magnetic fields, in order to

Contributed by the Design Engineering Division of ASME for publication in the JOURNAL OF VIBRATION AND ACOUSTICS. Manuscript received April 21, 2012; final manuscript received October 26, 2012; published online March 28, 2013. Assoc. Editor: Mahmoud Hussein.

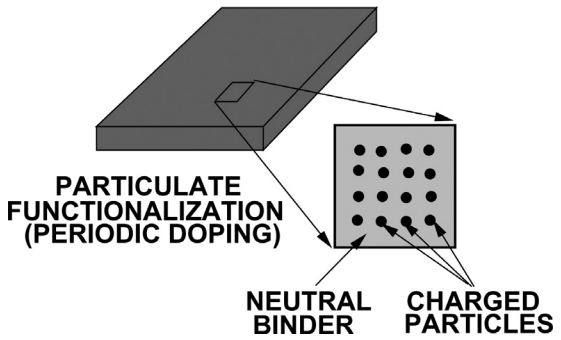

Fig. 1 A base, electromagnetically-neutral, solid that is doped with electromagnetically-sensitive particulates

qualitatively understand the individual electromagnetic and mechanical contributions, we consider three *single-particle* cases:

- Case 1: static electric and static magnetic fields acting on a single particle
- Case 2: static electric and static magnetic fields acting on a single particle that is bound ("tethered") to a point in space
- Case 3: oscillatory electric and static magnetic fields acting on a single particle that is bound to a point in space.

We recall the following important observation conjunction with electromagnetic phenomena (Jackson [43]):

- If a point charge (q) is in an electric field, **E**, it experiences an electrically-induced force, $\boldsymbol{\Psi}^e = q\boldsymbol{E}$.
- If a point charge is moving in a magnetic field, **B**, it experiences a magnetically-induced force, $\boldsymbol{\Psi}^m = qv \times \boldsymbol{B}$.
- If the fields occur simultaneously, then the electromagnetic force on the point charge is $\boldsymbol{\Psi}^{em} = q\boldsymbol{E} + qv \times \boldsymbol{B}$.

We consider an isolated charged mass with position vector denoted by **r**, governed by ($\dot{\boldsymbol{r}} = v, \ddot{\boldsymbol{r}} = \dot{v}$)

$$m\dot{v} = q(\boldsymbol{E} + v \times \boldsymbol{B}) \tag{2}$$

The governing Eq. (2), written in component form is, for component 1:

$$\dot{v}_1 = \frac{q}{m}(E_1 + (v_2B_3 - v_3B_2)) \tag{3}$$

for component 2:

$$\dot{v}_2 = \frac{q}{m}(E_2 - (v_1B_3 - v_3B_1)) \tag{4}$$

and for component 3:

$$\dot{v}_3 = \frac{q}{m}(E_3 + (v_1B_2 - v_2B_1)) \tag{5}$$

With the appropriate simplifications; for example that $\boldsymbol{E}^{\text{ext}} = (E_1^{\text{ext}}, E_2^{\text{ext}}, E_3^{\text{ext}})$ is an independent (not dependent on the particles) external electric field and $\boldsymbol{B}^{\text{ext}} = (B_1^{\text{ext}}, B_2^{\text{ext}}, B_3^{\text{ext}})$ is an independent external magnetic field.

(a) Case 1: static electric and static magnetic fields ($\boldsymbol{E}^{\text{ext}} = E_1^{\text{ext}}\boldsymbol{e}_1$ and $\boldsymbol{B}^{\text{ext}} = B^{\text{ext}}\boldsymbol{e}_3$) acting on a single particle.
In the special case when $\boldsymbol{r}(t=0) = \boldsymbol{0}$, $v(t=0) = \boldsymbol{0}$, $\boldsymbol{B}^{\text{ext}} = B_3^{\text{ext}}\boldsymbol{e}_3$ and $\boldsymbol{E}^{\text{ext}} = E_1^{\text{ext}}\boldsymbol{e}_1$, the governing equations are written in component form, for component 1:

$$\dot{v}_1 = \frac{q}{m}(E_1 + v_2B_3) \tag{6}$$

for component 2:

$$\dot{v}_2 = -\frac{q}{m}v_1B_3 \tag{7}$$

and for component 3:

$$\dot{v}_3 = 0 \tag{8}$$

The solution for the dynamics of an isolated particle is

$$\begin{Bmatrix} v_1(t) \\ v_2(t) \\ v_3(t) \end{Bmatrix} = \begin{Bmatrix} \frac{E_1^{\text{ext}}}{B_3^{\text{ext}}}\sin\omega t \\ \frac{E_1^{\text{ext}}}{B_3^{\text{ext}}}(\cos\omega t - 1) \\ 0 \end{Bmatrix} \Rightarrow \begin{Bmatrix} r_1(t) \\ r_2(t) \\ r_3(t) \end{Bmatrix} = \begin{Bmatrix} \frac{E_1^{\text{ext}}}{B_3^{\text{ext}}\omega}(1 - \cos\omega t) \\ \frac{E_1^{\text{ext}}}{B_3^{\text{ext}}}\left(\frac{\sin\omega t}{\omega} - t\right) \\ 0 \end{Bmatrix} \tag{9}$$

where $\omega = \left(qB_3^{\text{ext}}/m\right)$ is known as the cyclotron frequency. The cyclotron frequency ("gyrofrequency") is the angular frequency at which a charged particle makes circular orbits in a plane perpendicular to the static magnetic field. Notice that this traces out the equation of a "planar helix" with a radius parameter of

$$R = \frac{E_1^{\text{ext}}}{B_3^{\text{ext}}\omega} = \frac{mE_1^{\text{ext}}}{(B_3^{\text{ext}})^2 q} \tag{10}$$

in the $x_1 - x_2$ plane with x_1 coordinate fixed at $x_1 = \left(E_1^{\text{ext}}/B_3^{\text{ext}}\omega\right)$ that moves in the x_2 direction. We define the corresponding time period for one cycle to be completed as $T \stackrel{\text{def}}{=} 2\pi/\omega$. The basic trends are:

- as $B_3^{\text{ext}} \to \infty$ the radius shrinks at an inverse-quadratic rate and there is no motion
- as $E_1^{\text{ext}} \to \infty$ the radius grows at a linear rate
- as $m \to \infty$ the radius grows at a linear rate and
- as $q \to \infty$ the radius shrinks at an inverse linear rate

Remark. All the previous results collapse to those of classical mechanical vibrations when $B_3^{\text{ext}} = 0$. The approach is to differentiate the equation governing the first component, and then substitute the equation governing the second component and to solve a harmonic equation for the velocity of the first component, which is then used to generate the second component's solution. Both are then integrated in time to obtain the positions.

(b) Case 2: static electric and static magnetic fields acting on a single particle that is bound to a point in space.
Let us introduce a linear restoring force that tethers the particle in the x_1 direction, written in component form, for component 1:

$$\dot{v}_1 = \frac{q}{m}(E_1 + v_2B_3) - \frac{k_1r_1}{m} \tag{11}$$

where k_1 is a stiffness coefficient (Newtons/meter), and for component 2:

$$\dot{v}_2 = -\frac{q}{m}v_1B_3 \tag{12}$$

and for component 3:

$$\dot{v}_3 = 0 \tag{13}$$

The solution is

$$\begin{Bmatrix} v_1(t) \\ v_2(t) \\ v_3(t) \end{Bmatrix} = \begin{Bmatrix} \frac{qE_1^{\text{ext}}}{m\gamma}\sin\gamma t \\ \frac{\omega}{\gamma}\frac{qE_1^{\text{ext}}}{m\gamma}(\cos\gamma t - 1) \\ 0 \end{Bmatrix} \Rightarrow \begin{Bmatrix} r_1(t) \\ r_2(t) \\ r_3(t) \end{Bmatrix} = \begin{Bmatrix} \frac{qE_1^{\text{ext}}}{m\gamma^2}(1 - \cos\gamma t) \\ \frac{\omega}{\gamma}\frac{qE_1^{\text{ext}}}{m\gamma}\left(\frac{\sin\gamma t}{\gamma} - t\right) \\ 0 \end{Bmatrix} \tag{14}$$

where

$$\gamma = \sqrt{\omega^2 + \frac{k_1}{m}} \tag{15}$$

represents a shift of the cyclotronic natural frequency (ω). All the results in this section collapse to those of classical mechanical vibrations when $B_3^{\text{ext}} = 0$.

(c) Case 3: oscillatory electric and static magnetic fields acting on a single particle that is bound to a point in space. Introducing $E_1^{\text{ext}} = E_0^{\text{ext}}\sin\Omega t$, where E_0^{ext} is the amplitude, the solution is

$$\begin{Bmatrix} v_1(t) \\ v_2(t) \\ v_3(t) \end{Bmatrix} = \begin{Bmatrix} A(\cos\Omega t - \cos\gamma t) \\ A\omega\left(\frac{1}{\gamma}\sin\gamma t - \frac{1}{\Omega}\sin\Omega t\right) \\ 0 \end{Bmatrix} \tag{16}$$

and

$$\begin{Bmatrix} r_1(t) \\ r_2(t) \\ r_3(t) \end{Bmatrix} = \begin{Bmatrix} A\left(\frac{1}{\Omega}\sin\Omega t - \frac{1}{\gamma}\sin\gamma t\right) \\ A\omega\left(\frac{1}{\Omega^2}(\cos\Omega t - 1) - \frac{1}{\gamma^2}(\cos\gamma t - 1)\right) \\ 0 \end{Bmatrix} \tag{17}$$

where

$$A = \frac{q}{m}\left(\frac{E_0^{\text{ext}}\Omega}{\gamma^2 - \Omega^2}\right) \tag{18}$$

Clearly, resonance occurs at $\Omega = \gamma = \sqrt{\omega^2 + (k_1/m)}$. which yields unbounded solutions. Thus, one may be able to induce extremely large amplitudes with the appropriate electric and magnetic fields. *One important point is that there is an electromagnetic frequency that adds to the system response; in addition to a mechanical one, even in the case where magnetic load is static.*

Remark. Equation (17) indicates beatlike phenomena can occur. Recall, beatlike phenomena occurs when two harmonic forms are combined. For example, consider

$$r(t) = A\cos\omega t + A\cos(\omega + \Delta\omega)t \tag{19}$$

which can be rewritten as

$$r(t) = A\cos\omega t + A\cos(\omega + \Delta\omega)t = \underbrace{2A\left(\cos\frac{\Delta\omega}{2}t\right)}_{\text{time-varying-amplitude}}\cos\left(\omega + \frac{\Delta\omega}{2}\right)t \tag{20}$$

As we will see later for groups of particles, there will be fast scale cyclotron-induced motion and slow scale motion, which is mechanically-induced.

3 Modeling Coupled Multiparticle Systems

The objects in the system are assumed to be small enough to be considered (idealized) as point-mass particles. We consider a group of nonintersecting particles (N_p in total) and build on the previous works of Zohdi [44–52]. The equation of motion for the *ith* particle in a system is

$$m_i\ddot{\boldsymbol{r}}_i = \boldsymbol{\Psi}_i^{\text{tot}}(\boldsymbol{r}_1, \boldsymbol{r}_2, ..., \boldsymbol{r}_{N_p}) = \boldsymbol{\Psi}_i^{nf} + \boldsymbol{\Psi}_i^{\text{env}} \tag{21}$$

where $\mathbf{r}_i$ is the position vector of the *ith* particle and where $\boldsymbol{\Psi}_i^{\text{tot}}$ represents all forces acting on particle i, which is decomposed into the sum of forces due to near-field interaction ($\boldsymbol{\Psi}^{nf}$) and the surrounding environment ($\boldsymbol{\Psi}^{\text{env}}$)[1].

(a) Particle-to-particle "near-field" interaction. We recall that the force between two electrically charged particles is given by (Coulomb's law)

$$\boldsymbol{\Psi}_{ij}^{e} = \frac{q_i q_j}{4\pi\epsilon||\boldsymbol{r}_i - \boldsymbol{r}_j||^2}\boldsymbol{n}_{ij} \tag{22}$$

where $\boldsymbol{\Psi}_{ij}^{e}$ is the force acting between the particles, q_i is the charge of particle i, q_j is the charge of particle j, ϵ is the permittivity and $\boldsymbol{n}_{ij}$ is the normal direction, determined by the difference in the position vectors of the particles' centers, defined by

$$\boldsymbol{n}_{ij} \overset{\text{def}}{=} -\frac{\boldsymbol{r}_i - \boldsymbol{r}_j}{||\boldsymbol{r}_i - \boldsymbol{r}_j||} = \frac{\boldsymbol{r}_j - \boldsymbol{r}_i}{||\boldsymbol{r}_i - \boldsymbol{r}_j||} \tag{23}$$

where $||\boldsymbol{r}_i - \boldsymbol{r}_j||$ is the separation distance between particles i (located at $\boldsymbol{r}_i$) and j (located at $\boldsymbol{r}_j$) and $||\cdot||$ represents the Euclidean norm in R^3. Usually, one writes $\epsilon = \epsilon_o\epsilon_r$ where $\epsilon_o = 8.854 \times 10^{-12}$ farads/meter is the free space permittivity and ϵ_r is the relative permittivity or "dielectric" constant. For point charges of like sign, the Coulombic force is one of repulsion, while for opposite charges the force is attractive. Continuum formulations of Maxwell's equations could be applied at the scale, however, the system of numerical equations will become enormous. This is discussed at the end of the paper. For this reason, reduced-order, empirically-generated effective interaction laws for complex charged-particulate interaction, which possess attractive and repulsive components, are employed. Following Zohdi [44–52], a simple form that captures basic interaction characteristics is

$$\boldsymbol{\Psi}_i^{nf} = \sum_{j\neq i}^{N_p}\left(\underbrace{\alpha_{1ij}||\boldsymbol{r}_i - \boldsymbol{r}_j||^{-\beta_1}}_{\text{attraction}} - \underbrace{\alpha_{2ij}||\boldsymbol{r}_i - \boldsymbol{r}_j||^{-\beta_2}}_{\text{repulsion}}\right)\underbrace{\boldsymbol{n}_{ij}}_{\text{unit vector}} \tag{24}$$

where the α's and β's are empirical material parameters. We note that there are a variety of possible interparticle representations for charged particles. We refer the reader to Frenklach and Carmer [53], Haile [54], Hase [55], Rapaport [56], Torquato [57], Rechtsman et al. [58,59] and Zohdi [44–52] for overviews of the various representations for particle interaction, such as those based on Mie, Lennard–Jones, and Morse potentials (see

[1]Such forces can arise from surrounding medium and the external electromagnetic fields.

Moelwyn-Hughes [60] for reviews). Also, three-body terms can be introduced directly into the interparticle interaction (Stillinger [61]) or via termwise modifications to the two-body representations (Tersoff [62]).

Remark. In the Appendix, numerical techniques for accurately solving the coupled set of nonlinear differential equations that arise in Eq. (21), using an implicit temporally-adaptive trapezoidal time-stepping scheme, are discussed in detail.

(b) Particle-to-particle interaction "stiffness."

Some important qualitative information can be determined about the interaction law in Eq. (24), if we consider a linearization of a single nonlinear differential equation, describing the attraction and repulsion from the origin ($r_o = 0$) of the form[2]

$$m\ddot{r} = \Psi^{nf}(r) \tag{25}$$

where

$$\Psi^{nf}(r) = -\alpha_1 r^{-\beta_1} + \alpha_2 r^{-\beta_2} \tag{26}$$

Upon linearization of the nonlinear interaction relation about a point r_*,

$$\Psi^{nf}(r) \approx \Psi^{nf}(r_*) + \frac{\partial \Psi^{nf}}{\partial r}|_{r=r_*}(r - r_*) + \mathcal{O}(r - r_*)^2 \tag{27}$$

and normalizing the equations, we obtain

$$\ddot{r} + (\omega_n^*)^2 r = \frac{f^*(t)}{m} \tag{28}$$

where

$$\omega_n^* = \sqrt{\frac{-\frac{\partial \Psi^{nf}}{\partial r}|_{r=r_*}}{m}} \tag{29}$$

and where

$$f^*(t) = \Psi^{nf}(r_*) - \frac{\partial \Psi^{nf}}{\partial r}|_{r=r_*} r_* \tag{30}$$

For the specific interaction form chosen we have

$$\omega_n^* = \sqrt{\frac{-\alpha_1\beta_1 r_*^{-\beta_1-1} + \alpha_2\beta_2 r_*^{-\beta_2-1}}{m}} \tag{31}$$

and where the "loading" is

$$f^*(t) = -\alpha_1 r_*^{-\beta_1} + \alpha_2 r_*^{-\beta_2} - \alpha_1\beta_1 r_*^{-\beta_1-1} + \alpha_2\beta_2 r_*^{-\beta_2-1} \tag{32}$$

We note that if the following specific choice of parameters is made $(\beta_1, \beta_2) = (1, 2)$, and r_* is chosen as the static equilibrium point, r_e, where $\Psi^{nf}(r_e) = 0$, then $r_* = r_e = (\alpha_2/\alpha_1)$ and

$$\omega_n^* = \sqrt{\frac{\alpha_1\left(\frac{\alpha_1}{\alpha_2}\right)^2}{m}} \stackrel{\text{def}}{=} \sqrt{\frac{k^*}{m}} \tag{33}$$

where $k^* \stackrel{\text{def}}{=} \alpha_1(\alpha_1/\alpha_2)^2$ Thus, if we keep the ratio α_1/α_2 constant, while increasing α_1, we effectively increase the interaction "stiffnesses" between particles.

4 Numerical Examples: A Model Problem

We considered the response of a sample comprised of a $7 \times 7 \times 7$ periodic (cubic) array of particles in Fig. 2 embedded in a binding medium, due to external oscillatory loading. In this reduced-order model, the only role of the binding medium was to tether the particles to their original equilibrium ($t = 0$) positions. In the conclusions, a discussion of the extensions to modeling these systems as a continuum, where the binder deformation would be accounted for, is provided. As for the isolated, single particle example, for each particle, $v_i(t = 0) = \mathbf{0}$, $\boldsymbol{B}^{\text{ext}} = B_3^{\text{ext}}\boldsymbol{e}_3$ and $\boldsymbol{E}^{\text{ext}} = E_1^{\text{ext}}\boldsymbol{e}_1$, where $E_1^{\text{ext}} = E_0^{\text{ext}}\sin\Omega t$. The test parameters used in the example (where the domain is a 0.2m $\times$ 0.2m $\times$ 0.2m sized cube) were

- the masses of the particles: $m_i = \rho(4/3)\pi r_i^3$, where $\rho = 2000$ kg/m^3, $r_i = 0.005$ m
- for the particle-to-particle interaction law: $(\alpha_1, \beta_1, \alpha_2, \beta_2) = (2, 1, 1, 2)$
- the charges of the particles: $q_i = 1$ C
- the static magnetic field: $B_3^{\text{ext}} = 1$ Tesla
- the oscillatory electric field amplitude: $E_0^{\text{ext}} = 0.1$ N/C
- the binding constant to the medium: $k = 0.5$ N/m

The overall response of the CG is shown in Fig. 3 for various responses to the values of the forcing frequencies below:

(a) $\Omega = 0.1\omega$
(b) $\Omega = 0.2\omega$
(c) $\Omega = 0.4\omega$
(d) $\Omega = 0.8\omega$
(e) $\Omega = 1.0\omega$ (near cyclotronic resonance)
(f) $\Omega = 1.2\omega$
(g) $\Omega = 1.4\omega$ and
(h) $\Omega = 1.8\omega$

For this specific example, the following quantities are important:

- cyclotronic contribution: $\omega = qB/m = 1819.38531/s$ (for this example)

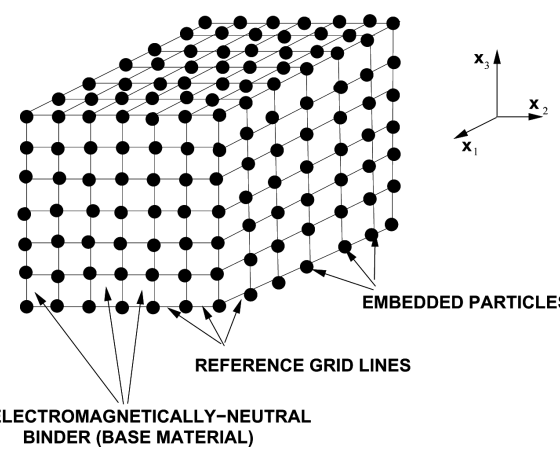

Fig. 2 The model problem for the numerical simulation. It is a periodic array of 7×7×7 charged particles embedded in a binding medium, due to external oscillatory loading. As for the isolated, single particle example, for each particle, $v_i(t = 0) = 0$, $B^{\text{ext}} = B_3^{\text{ext}}e_3$ and $E^{\text{ext}} = E_1^{\text{ext}}e_1$, where $E_1^{\text{ext}} = E_0^{\text{ext}}\sin\Omega t$.

[2]The unit normal has been taken into account; thus the presence of a change in sign.

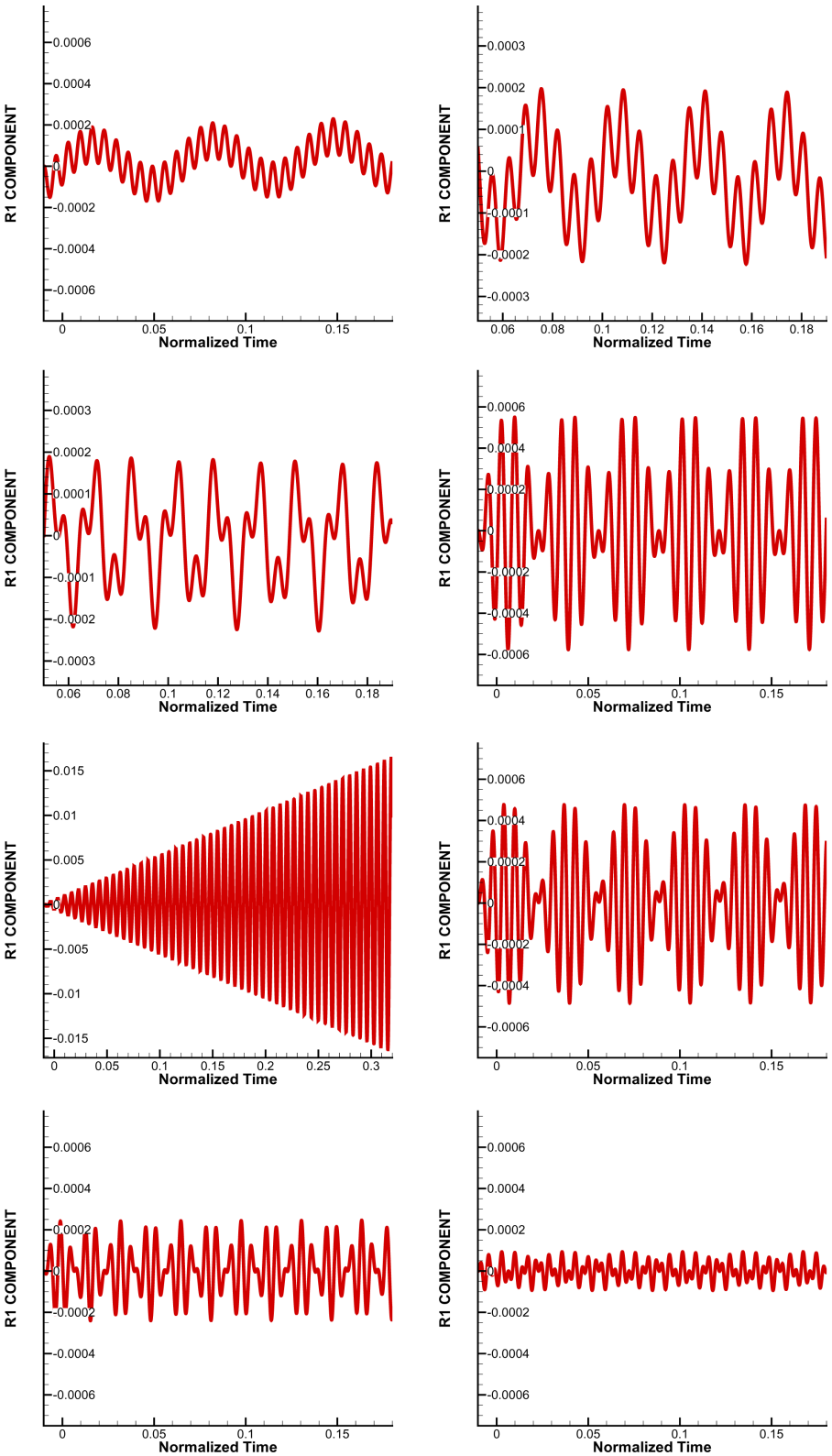

Fig. 3 Various responses of the CG of the sample to the values of the forcing frequency, left to right and top to bottom: (*a*) $\Omega = 0.1\omega$, (*b*) $\Omega = 0.2\omega$, (*c*) $\Omega = 0.4\omega$, (*d*) $\Omega = 0.8\omega$, (*e*) $\Omega = 1.0\omega$ (very near to resonance), (*f*) $\Omega = 1.2\omega$, (*g*) $\Omega = 1.4\omega$ and (*h*) $\Omega = 1.8\omega$. Note that as for the isolated, single particle example, for each particle, $v_i(t = 0) = 0$, $B^{\text{ext}} = B_3^{\text{ext}} e_3$ and $E^{\text{ext}} = E_1^{\text{ext}} e_1$, where $E_1^{\text{ext}} = E_0^{\text{ext}} \sin\Omega t$.

- binding contribution: $\sqrt{k/m} = 21.85091/s$ (k is the medium's stiffness), where

$$\boldsymbol{\Psi}_i^b = (k(\boldsymbol{r}_{i1} - \boldsymbol{r}_{i1}(t=0)),\ k(\boldsymbol{r}_{i2} - \boldsymbol{r}_{i2}(t=0)),\ k(\boldsymbol{r}_{i3} - \boldsymbol{r}_{i3}(t=0))) \tag{34}$$

- combined terms: $\sqrt{\omega^2 + k/m} = 1819.51651/s$
- particle-to-particle contribution: $\omega_n^* = \sqrt{\alpha_1(\alpha_1/\alpha_2)^2/m} = 87.4038\ 1/s$

Notably, the oscillatory nature of $\boldsymbol{E}^{\text{ext}}$ induces mechanical and electromagnetic responses. As Ω approaches the cyclotronic frequency, the vibrations grow dramatically, as seen in the plot in Fig. 3 for $\Omega = \omega$. As one may observe in Fig. 3, "beat" phenomena occurs in all cases, due to the combinations of harmonics that arise from the mechanical binding, electromagnetic field and near-field interaction. In particular, for the parameter sets chosen, it is observed that the fast cyclotronic vibration can be attributed to the magnetic field and there are two slow "restoring" frequencies from (a) the medium and (b) the particle-to-particle near-field interaction (Eq. (20)). *It is important to emphasize that, with the applied numerical scheme (see Appendix), the formulation provided in this paper is general enough to consider random distributions of particles.*

5 Closing Comments and Extensions

For the considered material systems, more complex continuum models are clearly possible, and may be necessary in certain applications. However, such models are extremely computationally-intensive, since the entire medium must be discretized with a spatial mesh, leading to a huge number of equations. For example, for a continuum formulation, in order to accurately capture the coupled (time-transient) electromagnetic and mechanical behavior, in particular Joule-heating, of a particle-laden material, Zohdi [63] developed a staggered temporally-adaptive finite difference time domain (FDTD) method that resolved the continuum electric, magnetic and mechanical fields throughout the material. Several million spatial grid points were needed to compute the fields accurately, for samples of materials containing a only a few hundred particles in a binding matrix. Other direct numerical simulation approaches are also applicable, and may have advantages over one another, depending on the material microstructure and the specific physics involved. Such methods include: (a) *the Multi-Resolution Time Domain Method*, which is based on wavelet-based discretization, (b) *the Finite Element Method*, which is based on discretization of variational formulations and which are well-suited for irregular geometries, (c) *the Pseudo Spectral Time Domain Method*, which is based on Fourier and Chebyshev transforms, followed by a lattice or grid discretization of the transformed domain (d) *the Discrete Dipole Approximation*, which based on an array of dipoles solved iteratively with the Conjugate Gradient method and a Fast Fourier Transform to multiply matrices, (e) *the Method of Moments*, which is based on integral formulations employing Boundary Element Method discretization, often accompanied by the Fast Multipole Method to accelerate summations needed during the calculations and (f) *the Partial Element Equivalent Circuit Method*, which is based on integral equations that are interpreted as circuits in discretization cells. The development of robust numerical methods, utilizing methods (a)–(f), in conjunction with FDTD, is under current investigation by the author, for continuum formulations of the vibrational particle-laden systems studied in this paper.

Appendix: Numerical Methods: Time-Stepping and Adaptive Recursion

Integrating Eq. (21) leads to (a trapezoidal rule with $0 \leq \varphi \leq 1$)

$$\begin{aligned} v_i(t+\Delta t) &= v_i(t) + \frac{1}{m_i}\int_t^{t+\Delta t} \boldsymbol{\Psi}_i^{\text{tot}} dt \\ &= v_i(t) + \frac{1}{m_i}\left(\int_t^{t+\Delta t} (\boldsymbol{\Psi}_i^{nf} + \boldsymbol{\Psi}_i^{\text{env}}) dt\right) \\ &\approx v_i(t) + \frac{\Delta t}{m_i}\Big(\phi(\boldsymbol{\Psi}_i^{nf}(t+\Delta t) + \boldsymbol{\Psi}_i^{\text{env}}(t+\Delta t)) \\ &\quad + (1-\phi)(\boldsymbol{\Psi}_i^{nf}(t) + \boldsymbol{\Psi}_i^{\text{env}}(t))\Big) \end{aligned} \tag{A1}$$

The position can be computed via

$$\begin{aligned} \boldsymbol{r}_i(t+\Delta t) &= \boldsymbol{r}_i(t) + v_i(t)\Delta t + \frac{\phi(\Delta t)^2}{m_i} \\ &\quad \times \Big(\phi(\boldsymbol{\Psi}_i^{nf}(t+\Delta t) + \boldsymbol{\Psi}_i^{\text{env}}(t+\Delta t)) \\ &\quad + (1-\phi)(\boldsymbol{\Psi}_i^{nf}(t) + \boldsymbol{\Psi}_i^{\text{env}}(t))\Big) \end{aligned} \tag{A2}$$

Remark. Generally speaking, if a recursive process is *not employed* (an explicit scheme), the iterative error can accumulate rapidly. However, an overkill approach involving very small time steps, smaller than needed to control the discretization error, simply to suppress a nonrecursive process error, is computationally inefficient. This is discussed next.

(a) Iterative (implicit) solution method.

We now formulate an adaptive iterative scheme by building on an approach found in various forms in Zohdi [44–52]. We write Eq. (A2) in a slightly more streamlined form for particle i:

$$\begin{aligned} \boldsymbol{r}_i^{L+1} &= \boldsymbol{r}_i^L + v_i^L\Delta t + \frac{\phi\Delta t}{m_i} \\ &\quad \times \left(\Big(\phi(\boldsymbol{\Psi}_i^{nf,L+1} + \boldsymbol{\Psi}_i^{\text{env},L+1}) + (1-\phi)(\boldsymbol{\Psi}_i^{nf,L} + \boldsymbol{\Psi}_i^{\text{env},L})\Big)\Delta t\right) \end{aligned} \tag{A3}$$

which leads to a coupled set equations for $i = 1, 2, ..., N_p$ particles[3]. The set of equations represented by Eq. (A3) can be solved recursively. Equation (A3) can be solved recursively by recasting the relation as

$$\begin{aligned} \boldsymbol{r}_i^{L+1,K} &= \underbrace{\boldsymbol{r}_i^L + v_i^L\Delta t + \frac{\phi(\Delta t)^2}{m_i}\Big((1-\phi)(\boldsymbol{\Psi}_i^{nf}(\boldsymbol{r}^L) + \boldsymbol{\Psi}_i^{\text{env}}(\boldsymbol{r}^L))\Big)}_{\mathcal{R}} \\ &\quad + \underbrace{\frac{\phi(\Delta t)^2}{m_i}\Big(\varphi(\boldsymbol{\Psi}_i^{nf,L+1,K-1} + \boldsymbol{\Psi}_i^{\text{env},L+1,K-1})\Big)}_{\mathcal{G}(\boldsymbol{r}_i^{L+1,K-1})}, \end{aligned} \tag{A4}$$

where

$$\boldsymbol{\Psi}_i^{nf\ \text{or env},L} \overset{\text{def}}{=} \boldsymbol{\Psi}_i^{nf\ \text{or env},L}(\boldsymbol{r}_1^L, \boldsymbol{r}_2^L, ..., \boldsymbol{r}_N^L) \tag{A5}$$

and

$$\boldsymbol{\Psi}_i^{nf\ \text{or env},L+1,K-1} \overset{\text{def}}{=} \boldsymbol{\Psi}_i^{nf\ \text{or env},L+1,K-1}(\boldsymbol{r}_1^{L+1,K-1}, \boldsymbol{r}_2^{L+1,K-1}, ..., \boldsymbol{r}_N^{L+1,K-1}) \tag{A6}$$

which is of the form $\boldsymbol{r}_i^{L+1,K} = \mathcal{G}(\boldsymbol{r}_i^{L+1,K-1}) + \mathcal{R}_i$, where $K = 1, 2, 3, ...$ is the index of iteration within time step $L+1$ and $\mathcal{R}_i$ is a remainder term that does not depend on the solution. The convergence of such a scheme is dependent on the behavior of $\mathcal{G}$. Namely, a sufficient condition for convergence is that $\mathcal{G}$ is a contraction mapping for all $\boldsymbol{r}_i^{L+1,K}, K = 1, 2, 3, ...$ In order to investigate this further, we define the iteration error as

[3]The superscript L is a time interval counter.

$$\varpi_i^{L+1,K} \overset{\text{def}}{=} \boldsymbol{r}_i^{L+1,K} - \boldsymbol{r}_i^{L+1} \tag{A7}$$

A necessary restriction for convergence is iterative self consistency, i.e., the "exact" (discretized) solution must be represented by the scheme, $\boldsymbol{r}_i^{L+1} = \mathcal{G}(\boldsymbol{r}_i^{L+1}) + \mathcal{R}_i$. Enforcing this restriction, a sufficient condition for convergence is the existence of a contraction mapping

$$\left\| \underbrace{\boldsymbol{r}_i^{L+1,K} - \boldsymbol{r}_i^{L+1}}_{\varpi_i^{L+1,K}} \right\| = \left\| \mathcal{G}(\boldsymbol{r}_i^{L+1,K-1}) - \mathcal{G}(\boldsymbol{r}_i^{L+1}) \right\| \leq \eta^{L+1,K} \left\| \boldsymbol{r}_i^{L+1,K-1} - \boldsymbol{r}_i^{L+1} \right\| \tag{A8}$$

where, if $0 \leq \eta^{L+1,K} < 1$ for each iteration K, then $\varpi_i^{L+1,K} \to \mathbf{0}$ for any arbitrary starting value $\boldsymbol{r}_i^{L+1,K=0}$, as $K \to \infty$, which is a contraction condition that is sufficient, but not necessary, for convergence. The convergence of Eq. (A4) is scaled by $\eta \propto [(\varphi \Delta t)^2 / m_i]$. Therefore, we see that the contraction constant of $\mathcal{G}$ is (1) directly dependent on the strength of the interaction forces ($||\boldsymbol{\Psi}||$), (2) inversely proportional to m_i and (3) directly proportional to $(\Delta t)^2$ (at time $= t$). Thus, decreasing the time step size improves the convergence. *In order to simultaneously maximize the time step sizes to decrease overall computing time, while still meeting an error tolerance on the numerical solution's accuracy*, we build on an approach found in Zohdi [44] originally developed for continuum thermo-chemical multifield problems, in which one approximates $\eta^{L+1,K} \approx S(\Delta t)^p$, ($S$ is a constant) and one assumes that the error within an iteration to behave according to $(S(\Delta t)^p)^K \varpi^{L+1,0} = \varpi^{L+1,K}, \quad K = 1, 2, ..., \quad$ where $\varpi^{L+1,0} = \boldsymbol{r}^{L+1,K=1} - \boldsymbol{r}^L$ is the initial norm of the iterative (relative) error and S is intrinsic to the system, where; for example, for the class of problems under consideration, due to the quadratic dependency on Δt, $p \approx 2$. Our goal is to meet an error tolerance in exactly a preset (the analyst sets this) number of iterations. To this end, one writes $(S(\Delta t_{\text{tol}})^p)^{K_d} \varpi^{L+1,0} = TOL$, where TOL is a tolerance and where K_d is the number of desired iterations. If the error tolerance is not met in the desired number of iterations, the contraction constant $\eta^{L+1,K}$ is too large. Accordingly, one can solve for a new smaller step size, under the assumption that S is constant,

$$\Delta t_{\text{tol}} = \Delta t \left(\frac{\left(\frac{TOL}{\varpi^{L+1,0}}\right)^{\frac{1}{pK_d}}}{\left(\frac{\varpi^{L+1,K}}{\varpi^{L+1,0}}\right)^{\frac{1}{pK}}} \right) \tag{A9}$$

The assumption that S is constant is not critical, since the time steps are to be recursively refined and unrefined throughout the simulation. Clearly, the expression in Eq. (A9) can also be used for time step enlargement, if convergence is met in less than K_d iterations (typically chosen to be between five to ten iterations). Specifically, the solution steps are, within a time step:

(1) start a global fixed iteration (set $i = 1$ and $K = 1$)
(2) if $i > N_p$ then go to (4)
(3) if $i \leq N_p$ then:
  (a) compute the position $\mathbf{r}_i^{L+1,K}$
  (b) go to (2) for the next particle ($i = i + 1$)

(4) measure error (normalized) quantities
  (a) $\varpi_K \overset{\text{def}}{=} \frac{\sum_{i=1}^{N_p} ||\boldsymbol{r}_i^{L+1,K} - \boldsymbol{r}_i^{L+1,K-1}||}{\sum_{i=1}^{N_p} ||\boldsymbol{r}_i^{L+1,K} - \boldsymbol{r}_i^{L}||}$
  (b) $Z_K \overset{\text{def}}{=} \frac{\varpi_K}{TOL}$
  (c) $\Phi_K \overset{\text{def}}{=} \left(\frac{\left(\frac{TOL}{\varpi_0}\right)^{\frac{1}{pK_d}}}{\left(\frac{\varpi_K}{\varpi_0}\right)^{\frac{1}{pK}}} \right)$

(5) if the tolerance is met: $(Z_K \leq 1)$ and $K < K_d$ then
  (a) increment time: $t = t + \Delta t$
  (b) construct the next time step: $(\Delta t)^{\text{new}} = \Phi_K (\Delta t)^{\text{old}}$
  (c) select the minimum size: $\Delta t = \text{MIN}((\Delta t)^{\text{lim}}, (\Delta t)^{\text{new}})$ and go to (1)

(6) if the tolerance is not met: $(Z_K > 1)$ and $K < K_d$ then
  (a) update the iteration: $K = K + 1$
  (b) reset the particle counter: $i = 1$
  (c) go to (2)

(7) if the tolerance is not met $(Z_K > 1)$ and $K = K_d$ then
  (a) construct a new time step: $\Delta t = \Phi_K \Delta t$
  (b) restart at time t and go to (1)

Time step size adaptivity is critical, since the system's dynamics and configuration can dramatically change over the course of time, possibly requiring quite different time step sizes to control the iterative error. However, to maintain the accuracy of the time-stepping scheme, one must respect an upper bound dictated by the discretization error, i.e., $\Delta t \leq \Delta t^{\text{lim}}$. Note that in step (5), Φ_K may enlarge the time step if the error is lower than the preset tolerance.

References

[1] Maxwell, J. C., 1867, "On the Dynamical Theory of Gases," Philos. Trans. R. Soc. London **157**, pp. 49–88.
[2] Maxwell, J. C., 1873, *A Treatise on Electricity and Magnetism*, 3rd. ed., Clarendon, Oxford, UK.
[3] Rayleigh, J. W., 1892, "On the Influence of Obstacles Arranged in Rectangular Order Upon Properties of a Medium," Philos. Mag., **32**, pp. 481–491.
[4] Torquato, S., 2002, *Random Heterogeneous Materials: Microstructure and Macroscopic Properties*, Springer-Verlag, New York.
[5] Jikov, V. V., Kozlov, S. M., and Olenik, O. A., 1994, *Homogenization of Differential Operators and Integral Functionals*, Springer-Verlag, New York.
[6] Hashin, Z., 1983, "Analysis of Composite Materials: A Survey," ASME J. Appl. Mech., **50**, pp. 481–505.
[7] Markov, K. Z., 2000, "Elementary Micromechanics of Heterogeneous Media," *Heterogeneous Media: Micromechanics Modeling Methods and Simulations*, K. Z. Markov and L. Preziozi, eds., Birkhauser, Boston, pp. 1162.
[8] Mura, T., 1993, *Micromechanics of Defects in Solids*, 2nd ed., Kluwer, Dordrecht, Germany.
[9] Nemat-Nasser, S., and Hori, M., 1999, *Micromechanics: Overall Properties of Heterogeneous Solids*, 2nd ed., Elsevier, Amsterdam.
[10] Huet, C., 1982, "Universal Conditions for Assimilation of a Heterogeneous Material to an Effective Medium," Mech. Res. Commun., **9**(3): 165–170.
[11] Huet, C., 1984, "On the Definition and Experimental Determination of Effective Constitutive Equations for Heterogeneous Materials," Mech. Res. Commun., **11**(3), pp. 195–200.
[12] Zohdi, T. I., 2010, "On the Dynamics of Charged Electromagnetic Particulate Jets," Arch. Comput. Methods Eng., **17**(2), pp. 109–135.
[13] Zohdi, T. I., 2012, *Electromagnetic Properties of Multiphase Dielectrics: A Primer on Modeling, Theory and Computation*, Springer-Verlag, New York.
[14] Ghosh, S., 2011, *Micromechanical Analysis and Multi-Scale Modeling Using the Voronoi Cell Finite Element Method*, Taylor & Francis, London.
[15] Ghosh, S., and Dimiduk, D., 2011, *Computational Methods for Microstructure-Property Relations*, Springer New York.
[16] Rebeiz, G. M., Barker, N. S., Muldavin, J. B. and Tan, G. L., 2004, *Mechanical Modeling of MEMS Devices: Static Analysis RF MEMS: Theory, Design and Technology*, G.M. Rebeiz, ed., Wiley, New York, pp. 21–57.
[17] Quandt, E., and Ludwig, A., 2000, "Magnetorestrictive Actuation in Microsystems," Sens. Actuators **81**, pp. 275–280.
[18] Grimes, C., Ong, K., Loiselle, K., Stoyanov, P., Kouzoudis, D., Liu, Y., Tong, C., and Tefiku, F., 1999, "Magnetoelastic Sensors for Remote Query Environmental Monitoring," Smart Mater. Struct., **8**, pp. 639–646.
[19] Kouzoudis, D., and Grimes, C., 2000a, "The Frequency Response of Magnetoelastic Sensors to Stress and Atmospheric Pressure," Smart Mater. Struct., **9**, pp. 885–889.
[20] Kouzoudis, D., and Grimes, C., 2000b, "Remote Query Fluid Flow Velocity Measurement Using Magnetoelastic Thick Film Sensors," J. Appl. Phys., **87**(9), pp. 6301–6303.
[21] Azevedo, R. G., Jones, D. G., Jog, A. V., Jamshidi, B., Myers, D. R., Chen, L., Fu, X.A., Mehregany, M., Wijesundara, M.B.J. and Pisano, A.P., 2007, "A SiC MEMS Resonant Strain Sensor for Harsh Environment Applications," IEEE Sens. J., **7**(4), pp. 568–576.
[22] Jones, D. G., Azevedo, R. G., Chan, M. W., Pisano, A. P., and Wijesundara, M. B. J., 2007, "Low Temperature Ion Beam Sputter Deposition of Amorphous Silicon Carbide for Wafer-Level Vacuum Sealing," Proceedings of the IEEE 20th International Conference on Micro Electro Mechanical Systems (MEMS), Kobe, Japan, January 21–25.
[23] Myers, D. R., Cheng, K. B., Jamshidi, B., Azevedo, R. G., Senesky, D. G., Chen, L., Mehregany, M., Wijesundara, M. B. J., and Pisano, "A.P.A Silicon

Carbide Resonant Tuning Fork for Micro-Sensing Applications in High Temperature and High G-Shock Environments," J. Micro/Nanolith, MEMS MOEMS, **8**(2), p. 021116.
[24] Yamaguchi, M., Baba, M., Suezawa, K., Moizumi, T., Arai, K. I., Haga, A., Shimada, Y., Tanabe, S., and Itoh, K., 2000, "Improved RF Integrated Magnetic Thin-Film Inductors by Means of Micro Slits and Surface Planarization Techniques," IEEE Trans. Magn., **36**, pp. 3495–3498.
[25] Yamaguchi, M., Baba, M., and Arai, K. I., 2001, "Sandwich-Type Ferromagnetic RF Integrated Inductor," IEEE Trans. Microwave Theory Tech., **49**, pp. 2331–2335.
[26] Yamaguchi, M., Bae, S., Kim, K. H., Tan, K., Kusumi, T., and Yamakawa, K., 2005. "Ferromagnetic RF Integrated Inductor With Closed Magnetic Circuit Structure," IEEE MTT-S International Microwave Symposium Digest, Long Beach, CA, June 12–17, pp. 351–354.
[27] Zhuang, Y., Vroubel, M., Rejaei, B., and Burghartz, J. N., 2002, "Ferromagnetic RF Inductors and Transformers for Standard CMOS/BiCMOS," International Electron Devices Meeting (IEDM '02), San Francisco, CA, December 8–11, pp. 475–478.
[28] Zhuang, Y., Vroubel, M., Rejaei, B., Burghartz, J. N., and Attenborough, K., 2005, "Magnetic Properties of Electroplated Nano/Microgranular NiFe Thin Films for RF Application," J. Appl. Phys., **97**, p. 10N305.
[29] Zhuang, Y., Rejaei, B., Boellaard, E., Vroubel, M., and Burghartz, J. N., 2003, "Solenoid Inductors With Patterned, Sputter-Deposited Cr/$Fe_{10}Co_{90}$/Cr Ferromagnetic Cores," IEEE Electron Device Lett., **24**, pp. 224–226.
[30] Kim, G., Cha, S. Y., Hyun, E. K., Jung, Y., Choi, Y., Rieh, J. S., Lee, S. R., and Hwang, S., 2008, "Integrated Planar Spiral Inductors With CoFe and NiFe Ferromagnetic Layer," Microwave Opt. Technol. Lett., **50**, pp. 676–678.
[31] Gardner, D. S., Schrom, G., Hazucha, P., Paillet, F., Karnik, T., Borkar, S., Saulters, J., Owens, J., and Wetzel, J., 2006, "Integrated On-Chip Inductors With Magnetic Films," IEEE International Electron Devices Meeting (IEDM '06), San Francisco, CA, December 11–13, pp. 1–4.
[32] Gardner, D. S., Schrom, G., Hazucha, P., Paillet, F., Karnik, T. and Borkar, S., 2007, "Integrated On-Chip Inductors Design of Magnetic Medium Material and Fully-Closed With Magnetic Films," IEEE Trans. Magn., **43**, pp. 2615–2617.
[33] Viala, B., Royet, A. S., Cuchet, R., Ad, M., Gaud, P., Valls, O., Ledieu, M., and Acher O., 2004, "RF Planar Ferromagnetic Inductors on Silicon," IEEE Trans. Magn., **40**, pp. 1999–2001.
[34] Viala, B., Couderc, S., Royet, A.S., Ancey, P., and Bouche, G., 2005, "Bidirectional Ferromagnetic Spiral Inductors Using Single Deposition," IEEE Trans. Magn., **41**, pp. 3544–3549.
[35] Xu, W., Sinha, S., Pan, F., Dastagir, T., Cao, Y., and Yu, H., 2010, "Improved Frequency Response of On-Chip Inductors With Patterned Magnetic Dots," IEEE Electron Device Lett., **31**, pp. 207–209.
[36] Jiang, R. F., Shams, N. N., Rahman, M. T., and Lai, C. H., 2007, "Exchange-Coupled IrMn/CoFe Multilayers for RF-Integrated Inductors," IEEE Trans. Magn., **43**, pp. 3930–3932.
[37] Ikeda, K., Kobayashi, K., Ohta, K., Kondo, R., Suzuki, T., and Fujimoto, M., 2003, "Thin-Film Inductor for Gigahertz Band With CoFeSiO-SiO_2 Multilayer Granular Films and Its Application for Power Amplifier Module," IEEE Trans. Magn., **39**, pp. 3057–3061.
[38] Zhao, J., Zhu, J., Chen, Z., and Liu, Z., 2005, "Radio-Frequency Planar Integrated Inductor With Permalloy Granular Films," IEEE Trans. Magn., **41**, pp. 2334–2338.
[39] Hsu, M. C., Chao, T. Y., Cheng, Y. Y., Liu, C. M., and Chen, C., 2009, "The Inductance Enhancement Study of Spiral Inductor Using Ni–AAO Nanocomposite Core," IEEE Trans. Nanotechnol., **8**, pp. 281–285.
[40] Salvia, J., Bain, J. A., and Patrick Yue, C., 2005, "Tunable On-Chip Inductors Up to 5 GHz Using Patterned Permalloy Laminations," IEEE International Electron Devices Meeting, IEDM Technical Digest, Washington, DC, December 5, pp. 943–946.
[41] Rousselle, D., Berthault, A., Acher, O., Bouchaud, J. P., and Zrah, P. G., 1993, Effective Medium at Finite Frequency: Theory and Experiment, J. Appl. Phys., **74**, pp. 475–479.
[42] Wallace, L., 1993, "Broadband Magnetic Microwave Absorbers: Fundamental Limitations," IEEE Trans. Magn., **29**, pp. 4209–4214.
[43] Jackson, J. D., 1998, *Classical Electrodynamics*, 3rd ed., Wiley, New York.
[44] Zohdi, T. I., 2002, "An Adaptive-Recursive Staggering Strategy for Simulating Multifield Coupled Processes in Microheterogeneous Solids," Int. J. Numer. Methods Eng., **53**, pp. 1511–1532.
[45] Zohdi, T. I., 2004, "Modeling and Direct Simulation of Near-Field Granular Flows," Int. J. Solids Struct., **42**(2), pp 539–564.
[46] Zohdi, T. I., 2004, "A Computational Framework for Agglomeration in Thermo-Chemically Reacting Granular Flows," Proc. Royal Soc., **460**(2052), pp. 3421–3445.
[47] Zohdi, T. I., 2005, "Charge-Induced Clustering in Multifield Particulate Flow," Int. J. Numer. Methods Eng., **62**(7), pp. 870–898.
[48] Zohdi, T. I., 2007, "Computation of Strongly Coupled Multifield Interaction in Particle-Fluid Systems," Comput. Meth. Appl. Mech. Eng., **196**, pp. 3927–3950.
[49] Zohdi, T. I., 2007, *Introduction to the Modeling and Simulation of Particulate Flows*, SIAM, Philadelphia, PA.
[50] Zohdi, T. I. and Wriggers, P., 2008, *Introduction to Computational Micromechanics*, Springer-Verlag, New York.
[51] Zohdi, T. I., "On the Dynamics of Charged Electromagnetic Particulate Jets," Arch. Comput. Methods Eng., **17**(2), pp. 109–135.
[52] Zohdi, T. I., 2012, *Dynamics of Charged Particulate Systems: Modeling, Theory and Computation*, Springer-Verlag, New York.
[53] Frenklach, M., and Carmer, C. S., 1999, "Molecular Dynamics Using Combined Quantum and Empirical Forces: Application to Surface Reactions," *Molecular Dynamics of Clusters, Surfaces, Liquids, and Interfaces* (Advances in Classical Trajectory Methods), Vol. IV, W. L. Hase, ed., JAI Press, Stamford, CT, pp. 27–63.
[54] Haile, J. M., 1992, *Molecular Dynamics Simulations: Elementary Methods*, Wiley, New York.
[55] Hase, W. L., ed., 1999, *Molecular Dynamics of Clusters, Surfaces, Liquids, & Interfaces* (Advances in Classical Trajectory Methods), Vol. 4, JAI Press, Greenwich, CT.
[56] Rapaport, D. C., 1995, *The Art of Molecular Dynamics Simulation*, Cambridge University, Cambridge, UK.
[57] Torquato, S., 2009, "Inverse Optimization Techniques for Targeted Self-Assembly," Soft Matter **5**, pp. 1157–1173.
[58] Rechtsman, M., Stillinger, F. H., and Torquato, S., 2006, "Designed Interaction Potentials Via Inverse Methods for Self-Assembly," Phys. Rev. E **73**, p. 011406.
[59] Rechtsman, M., Stillinger, F. H., and Torquato, S., 2005, "Optimized Interactions for Targeted Self-Assembly: Application to Honeycomb Lattice," Phys. Rev. Lett., **95**, p. 228301.
[60] Moelwyn-Hughes, E. A., 1961, *Physical Chemistry*, Pergamon, New York.
[61] Stillinger, F. H., and Weber, T. A., 1985, "Computer Simulation of Local Order in Condensed Phases of Silicon," Phys. Rev. B, **31**, pp. 5262–5271.
[62] Tersoff, J., 1988, "Empirical Interatomic Potential for Carbon, With Applications to Amorphous Carbon," Phys. Rev. Lett., **61**, pp. 2879–2882.
[63] Zohdi, T. I., 2010, "Simulation of Coupled Microscale Multiphysical-Fields in Particulate-Doped Dielectrics With Staggered Adaptive FDTD," Comput. Methods Appl. Mech. Eng., **199**, pp. 79–101.